Effect of Pore Width on Micropore Filling Mechanism of SO_2 in Carbon Micropores

Zheng-Ming Wang and Katsumi Kaneko*

Physical Chemistry, Material Science, Graduate School of Natural Science and Technology, Chiba University, Yayoi 1-33, Inage-ku, Chiba 263, Japan

Received: October 8, 1997; In Final Form: February 11, 1998

The mechanism of SO_2 micropore filling in slit-shaped micropores was examined by direct calorimetry and potential calculation, and the effect of the pore width on the SO_2 micropore filling mechanism is discussed. Four kinds of activated carbon fibers of different pore widths have been used, and both granular activated carbon and microporous Boehmite aggregates were used for comparison. The differential energy of SO_2 adsorption (q_d) on ACFs varied with change of the average pore width. An increase of the micropore width leads to a decrease of q_d in SO_2 micropore filling by decreasing the enhanced micropore field. Molecular potential calculations gave good agreement with the experimental adsorption energy when the image potential due to the SO_2 dipole moment was considered. The image potential contributes 25−32% to the total molecular potential, indicating its importance in micropore filling of dipolar SO_2.

Introduction

Micropore filling has been studied extensively over the last 30 years.[1−9] However, the relationship between the mechanism of micropore filling and molecular states upon micropore filling is not sufficiently elucidated. Direct calorimetry can provide useful information on the states of molecules adsorbed.[10−12] Hence, there has been active calorimetric research on micropore filling recently.[13−26] Also, newly developed computer simulation studies need calorimetric data on micropore filling of various kinds of molecules.[27−30]

Specific interaction should play an important role in the micropore filling of a polar molecule. There are many important polar molecules having large dipole moments. H_2O is a representative dipolar molecule. Recent in-situ X-ray diffraction studies showed that water molecules form an ordered structure in the carbon micropore, indicating that the contribution of hydrogen bonding is significant in the intermolecular interaction.[31,32] SO_2 has a large dipole moment and the adsorption on activated carbons has been studied with relevance to atmospheric environmental problems. As the intermolecular interaction of SO_2 has no contribution from hydrogen bonding, we can understand how the molecular dipole is associated with the micropore filling. In particular, activated carbon fibers (ACFs) have controlled uniform micropores,[33−39] and the micropore filling mechanism of SO_2 on the microporous carbon can be examined as a function of the pore width.

The preceding work using calorimetric measurement, and a molecular potential calculation for SO_2 adsorbed in the narrow slit pore, where only a single SO_2 layer can be filled, showed a dipole-oriented structure of SO_2.[40] The importance of the dipole−induced dipole interaction in the molecular surface interaction was indicated. Systematic examinations of SO_2 adsorption on various ACFs having different pore widths should provide a greater understanding of the micropore filling mechanism of the polar molecule. This study describes the effect of the micropore width on the micropore filling of SO_2 using the combined approaches of the calorimetric measurement and molecular potential calculation.

Experimental Section

Pitch-based ACFs (denoted as P10, P15, P20, and P25; Osaka Gas Co.), with micropore width increasing with the serial number, were used for this study. The granulated activated carbon (denoted as AC) from Takeda Yakushin Co. and Boehmite (γ-AlOOH) aggregates (denoted as BA) having slit-shaped micropores[41] were used for comparison. The microporosity of samples was determined by N_2 adsorption at 77 K. The SO_2 adsorption isotherms were determined gravimetrically at 303 K. The irreversible adsorption amounts of SO_2 were determined after evacuation during one night at 303 K. The differential adsorption energy of SO_2 on ACFs was measured by a standard twin-type calorimeter (Tokyo Richo Co.), having a high sensitivity of 28 mV/deg. A released heat, dQ_{int}, was determined, when dN_a molecules of SO_2 were adsorbed on a sample. Then, the differential adsorption energy, q_d, of SO_2 was calculated by the following equation:

$$q_d = (dQ_{int}/dN_a)_{T=303K} \quad (1)$$

Molecular Potential Calculation Method. The detailed calculation method of the interaction potential of a dipolar SO_2 molecule with the graphitic slit pore was described in our preceding work.[40] Here, we give a brief description. Physical characterizations of ACFs showed that ACF is composed of nanographites and the micropores can be approximated by the slit-shaped graphite pores.[37] Furthermore, ACF exhibits good semiconductivity.[42] The polar interaction of a SO_2 molecule with the graphitic slit pore, therefore, was calculated with the induced image potential method. The nonpolar interaction of SO_2 with the graphitic slit pore was calculated with the aid of the 10−4−3 potential proposed by Steele.[43] In the slit-shaped micropore, the nonpolar molecule−pore wall interactions from opposite pore walls are overlapped, as shown in eq 2:

S1089-5647(97)03270-7 CCC: $15.00
Published on Web 03/31/1998

$$\Psi_h(z_m) = 4\pi\rho\sigma_{sf}^2\Delta\epsilon_{sf}[(1/5)(\sigma_{sf}/(d - z_m))^{10} - (1/2)(\sigma_{sf}/(d - z_m))^4 - \sigma_{sf}^4/(6\Delta(0.61\Delta + d - z_m)^3)] + 4\pi\rho\sigma_{sf}^2\Delta\epsilon_{sf}[(1/5)(\sigma_{sf}/(d + z_m))^{10} - (1/2)(\sigma_{sf}/(d + z_m))^4 - \sigma_{sf}^4/(6\Delta(0.61\Delta + d + z_m)^3)] \quad (2)$$

where d is the distance between the nuclei of the first layer carbon atoms of the pore walls and the center of the micropore wall adsorbed molecule, and is calculated as the sum of half the pore width and the radius of carbon atom ($r_c = 0.071$ nm); z_m is the distance from the interacting center of an adsorbent molecule to the center of the pore; ρ is the number of carbon atoms per unit volume of a graphitic lattice; σ_{sf} and ϵ_{sf} are the distance contact and the potential well depth of a Lennard-Jones (LJ) potential between an adsorbent molecule and a carbon atom, respectively; and Δ is the intergraphitic layer distance. The σ_{sf} and ϵ_{sf} were calculated from the LJ parameters of SO_2 and a carbon atom by the Lorentz−Berthelot rule.[44] The following values of Δ, ρ, σ_{sf}, and ϵ_{sf} were used for the calculation: $\Delta = 0.335$ nm, $\rho = 11.36$ nm^{-3}, $\sigma_{sf} = 0.385$ nm, and $\epsilon_{sf} = 84$ K.

The polar molecule−slit pore interaction was calculated by the following equation with the image potential approximation:

$$\Psi_{mi}(z_m) = (-\mu^2/8)[1/(d - z_m - \Delta/2)^3 + 1/(d + z_m - \Delta/2)^3] \quad (3)$$

Here μ stands for the dipole moment of SO_2 ($\mu = 1.61$ D). The position of the image plane was assumed to be situated above the pore wall by $\Delta/2$ using Crowell's approximation for adsorption of SO_2 on the basal plane of the graphite.[45] The axis of the SO_2 dipole moment was assumed to be normal to the graphitic wall; that is, the maximum induced image potential was presumed. Summation of eqs 2 and 3 gives the total interaction potential of a SO_2 molecule with the graphitic micropore:

$$\Psi_t(z_m) = \Psi_h(z_m) + \Psi_{mi}(z_m) \quad (4)$$

From eq 4, the distance of the minimum potential, z_m*, and the minimum potential well depth, $\Psi(z_m$*), can be obtained. The total potential well depth Ψ_0 of a molecule with a single graphite surface was calculated; enhancement of the adsorption energy in the micropore is expressed by $\Psi(z_m$*)/Ψ_0.

Results and Discussion

Characterization of Samples. All of the N_2 adsorption isotherms of ACFs, AC, and BA were typical of type I. The micropore volume, $V_0(N_2)$, and the specific surface area, a_s, of ACF and AC were obtained from the α_s plot of the high-resolution N_2 adsorption isotherm based on the standard data of N_2 adsorption on nonporous carbon black;[37] that of BA was obtained from the α_s-plot analysis on nonporous oxides.[46] The average pore width w_m was obtained by geometrical calculation using $V_0(N_2)$ and a_s. These pore parameters are shown in Table 1. The pore width of ACF is in the range of 0.79−1.45 nm. The micropore volume and pore width of AC are similar to those of P10. However, AC has a wider pore size distribution than P10, because the adsorption isotherm at a low P/P_0 range was more gradual than that of P10. The pore width of BA, whose surface has a hydrophilic nature, is comparable to that of ACF or AC.

SO_2 Adsorption. Figure 1a shows the SO_2 adsorption isotherms on ACF samples. Here the amount of adsorption is normalized with the aid of the micropore volume from N_2 adsorption $V_0(N_2)$ and the amount of SO_2 adsorption $V(SO_2)$ using the bulk liquid density ($\rho_L(SO_2) = 1434$ Kg m^{-3} at the boiling point) ($f = V(SO_2)/V_0(N_2)$). The SO_2 adsorption isotherm of P5 in the preceding paper[40] is also shown for comparison. This figure shows distinctly the sensitive dependence of the adsorption isotherm on the pore width: the smaller the pore width, the sharper the uptake at a low P/P_0 region. Hence SO_2 adsorption needs a stronger interaction of a molecule with the pore. Although the adsorption isotherm of P5 belongs to type I, that of P25, having the widest pores, loses completely the nature of type I; rather, it is close to type III. The reason why the isotherm of P5 has the nature of type I was reported in the preceding paper.[40] In the case of P5 whose micropores can accept a single layer of SO_2, the contribution of a dipole−induced dipole interaction due to the dipole-oriented single layer structure gives the marked adsorption at a low P/P_0 region. As the adsorption isotherm of SO_2 on nonporous carbon black belongs to type III, the polar structure of SO_2 is not fit for adsorption of SO_2 on the graphitic surface. Then SO_2 molecules adsorbed in micropores of P25 have no ordered structure of dipoles intensifying the molecule−pore interaction. SO_2 molecules adsorbed in micropores of P10, P15, and P20 should lose the ordering of molecular dipoles in this order.

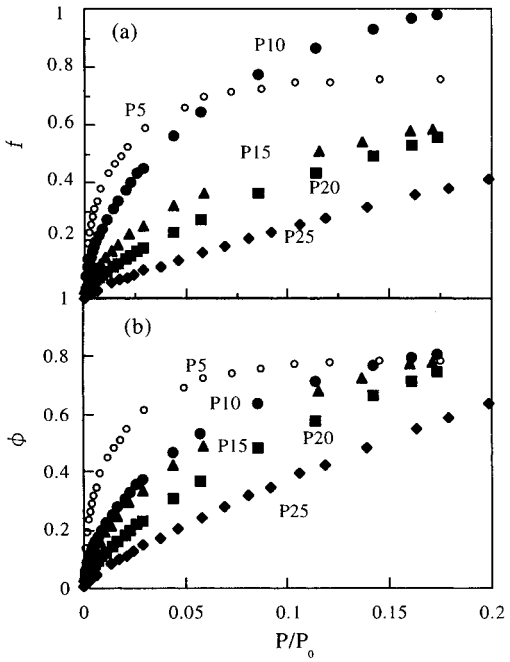

Figure 1. SO_2 adsorption isotherms of ACF samples with ordinates of (a) f and (b) ϕ.

TABLE 1: Microporosity of Samples

sample	P10	P15	P20	P25	AC	BA
$V_0(N_2)$/mL g^{-1}	0.753	0.767	0.971	1.344	0.514	0.24
a_s/m^2 g^{-1}	1190	1545	1765	1935	1250	360
w_m/nm	0.79	1.01	1.13	1.45	0.83	1.3

The Dubinin−Radushkevich (DR) equation was applied to the SO_2 adsorption isotherms. The DR equation is given by eq 5: [1−3]

$$\ln V(SO_2) = \ln V_0(SO_2) - (RT/\beta E_0(SO_2))^2 \ln^2 (P_0/P) \quad (5)$$

Here $V_0(SO_2)$ is the saturated SO_2 adsorption amount, P_0 is the saturated vapor pressure of SO_2 ($P_0 = 4.56 \times 10^5$ Pa at 303

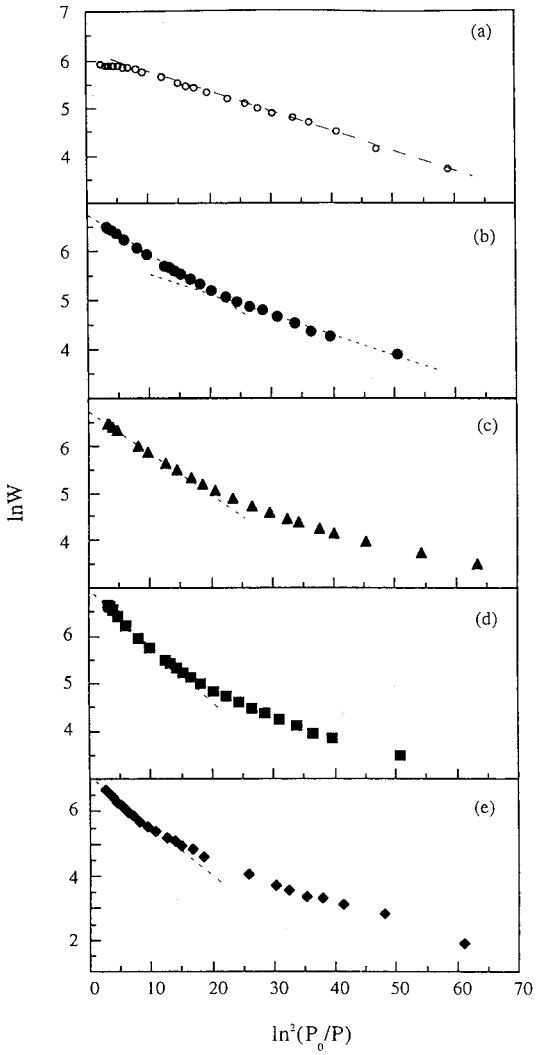

Figure 2. DR plots of SO_2 adsorption on ACF samples: (a) P5, (b) P10, (c) P15, (d) P20, (e) P25.

K), β is an affinity coefficient, and $E_0(SO_2)$ is the characteristic adsorption energy. If $V(SO_2)/V_0(SO_2)$ is expressed by ϕ (Figure 1b), the isosteric heat of adsorption of SO_2, $q_{st,\phi=1/e}$ at $\phi = 1/e$ is derived from both eq 5 and the Clausius−Clapeyron equation:[47]

$$q_{st,\phi=1/e} = \beta E_0(SO_2) + \Delta H_L \qquad (6)$$

Here ΔH_L is the condensation heat of the bulk SO_2 gas (ΔH_L = 24.9 kJ mol^{-1} at the boiling point). Figure 2 shows the DR plots of ACF samples. The DR plot of SO_2 on P5 has good linearity except for the high P/P_0 range. The DR plot of SO_2 on P10 is well expressed by two linear regions. Other DR plots for SO_2 are not expressed by the linear regions. As the DR plots for N_2 on these ACFs had a good linearity due to a well filling process of N_2 at 77 K, the nonlinear DR plots of SO_2 on P15, P20, and P25 suggest an incomplete filling of pores with SO_2 molecules. Accordingly, we cannot determine precisely the $V_0(SO_2)$ with the DR plot. Table 2 lists $V_0(SO_2)$ and $q_{st,\phi=1/e}$ determined from the DR plots in the high relative pressure range, and the SO_2 adsorption isotherms using ϕ as the ordinate are shown in Figure 1b. Table 2 also shows the ratio of $V_0(SO_2)$ to $V_0(N_2)$. Although $V_0(SO_2)$ increases with the pore width for PIT samples, both $q_{st,\phi=1/e}$ and $V_0(SO_2)/V_0(N_2)$ decreases with the pore width. Hence ACF samples having a larger pore width and a larger pore volume are not fit for SO_2 adsorption. Therefore, SO_2 molecules do not form well-ordered dipole-oriented structures in the micropores of P15, P20, and P25.

Figure 3 shows the adsorption isotherms of AC and BA in comparison with those of P5 and P25. The adsorption isotherms of SO_2 on both AC and BA are similar to that of P5. Although the pore width of BA is 1.3 nm, being close to that of P25, the SO_2 adsorption isotherm of BA rather resembles that of P5. This suggests that the interaction of SO_2 with the micropore of BA having surface hydroxyls is stronger than that with the graphitic pore. These SO_2 adsorption isotherms were analyzed with the DR equation. The $q_{st,\phi=1/e}$ of BA is larger than that of P20 or P25, although the micropore widths are close to each other. The surface hydroxyls on the slit pore walls of BA[41] should interact more effectively with the polar SO_2 molecule. Table 2 shows results for AC and BA. Both of ϕ and $q_{st,\phi=1/e}$ of AC are comparable to those of P5 due to the presence of narrower micropores. The ratios of the irreversible adsorption amounts of SO_2, $W_{irr}(SO_2)$, to $W_0(SO_2)$, are also shown in Table 2. The irreversible SO_2 adsorption is caused by the strong interaction of the SO_2 dipole with the local surface active sites. Hence, the larger W_{irr}/W_0 for SO_2 denotes the higher concentration of the surface functional groups. As the $W_{irr}(SO_2)/W_0(SO_2)$ of AC is very large, the SO_2 micropore filling on AC is affected by large amounts of surface functional groups. Among the ACF samples, only P10 shows a large value of $W_{irr}(SO_2)/W_0(SO_2)$ in comparison with P15−P25. We must take into account the presence of surface functional groups for P10, but the pore walls of P15−P25 can be presumed to be nonspecific. BA has a value of $W_{irr}(SO_2)/W_0(SO_2)$ comparable to that of P10, indicating a relatively weak specific interaction between dipolar SO_2 and surface functional groups due to defective structure as well as structural hydroxyl groups.

Experimental Adsorption Energy of SO_2 on Carbonaceous Micropore. Figure 4 shows the changes of differential adsorption energy, q_d, of SO_2 on ACF samples with ϕ. The broken line in the figures denotes the condensation heat of bulk SO_2 gas at the boiling point. The $q_d-\phi$ relation of P10 has two plateau regions in the ϕ range of 0.1 to 0.7. The large q_d below $\phi = 0.05$ should be ascribed to the presence of the surface functional groups. The $W_{irr}(SO_2)/W_0(SO_2)$ of 0.1 for P10 agrees well with the above result. The two plateau regions just coincide with the two linear regions in the DR plot. The corresponding q_d values are 37.0 and 33.0 kJ mol^{-1}. Hence these two plateau values come from the binodal micropore size distribution. The slight increase of q_d above $\phi = 0.7$ may be attributed to the enhanced intermolecular interaction which was distinctly observed in P5. The $q_d-\phi$ profile of P15 has a flat region below $\phi = 0.4$ and a gradual decrease at the higher ϕ region. The q_d value at the flat region is 36 kJ mol^{-1}, being slightly smaller than that of P10 at the first flat region. Therefore, the adsorption energy measurement indicates a similar SO_2 adsorption state for both P15 and P10 at the low ϕ region. As the adsorption energy depends on the micropore width, the micropore width of P15 corresponding to $\phi < 0.4$ should be close to that of P10 for the first plateau region. The gradual decrease of q_d in the larger ϕ region of P15 is ascribed to a wider pore size distribution than P10. P15 was prepared by a longer activation than P10, and the pore size distribution of P15 becomes wider. P20 and P25 have similar $q_d-\phi$ curves. Except for those in the low ϕ range, the q_d value is almost constant (<30 kJ mol^{-1}), being smaller than those of P10 and P15.

Figure 5a shows the change of differential adsorption energy of SO_2 on AC. The q_d of SO_2 adsorption below $\phi = 0.1$ is quite large (>40kJ/mol); this is attributed to the interaction of

TABLE 2: SO_2 Adsorption Data

sample	(P5)	P10	P15	P20	P25	AC	BA
$V_0(SO_2)$/mL g^{-1}	(0.32)	0.58	0.57	0.72	0.87	0.48	0.16
$q_{st,\phi=1/e}$/kJ mol^{-1}	(37.5)	33.9	33.6	32.2	30.8	35.3	33.6
$V_0(SO_2)/V_0(N_2)$	(0.95)	0.77	0.74	0.74	0.65	0.93	0.68
$W_{irr}(SO_2)/W_0(SO_2)$	(<0.1)	0.1	<0.01	<0.01	<0.01	0.32	0.10

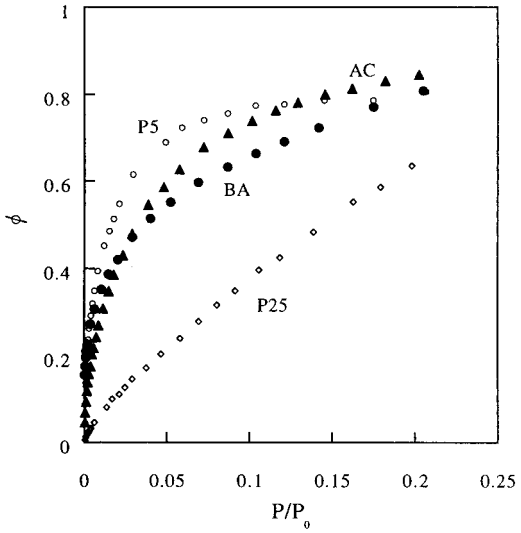

Figure 3. SO_2 adsorption isotherms on AC and BA.

SO_2 with the surface functional groups. The adsorption energy of SO_2 on AC at $\phi > 0.30$ is almost similar to the flat value of P10 in the larger ϕ range. Figure 5b shows the change of differential adsorption energy of SO_2 on BA with ϕ. The initial q_d value is very large (~70 kJ mol^{-1}) and it decreases gradually with ϕ. The change becomes steady around $\phi = 0.4$ and 0.6. The micropore wall of BA is composed of hydroxyls, and thereby the higher q_d value of BA must be ascribed to the electrostatic interaction of SO_2 with the ionic pore walls.

Molecular Potential Approaches to SO_2 in a Graphitic Pore. The above q_d data show that contribution of the interaction of SO_2 with surface functional groups can be neglected except for the very low ϕ region in the case of ACF. The molecular potential profiles of SO_2 with a graphitic slit pore as a function of pore width can provide important information on the micropore filling mechanism of SO_2 in micropores of ACF. The interaction potential profiles of a polar SO_2 molecule with the graphitic slit micropore calculated by eqs 2−4 are shown in Figure 6 for both cases with and without the dipole−induced dipole interaction. The dipole−induced dipole interaction contributes very much to stabilize the SO_2 molecule at the potential minimum; the contribution becomes larger with an increase of the pore width, because the dispersion interaction becomes smaller. Here the normal orientation of the dipole moments is necessary for the effective dipole−induced dipole interaction. Hence the oriented structure of the dipole moments of SO_2 is favored from the molecular potential. In particular, the dipole moments should be oriented with each other in micropores of P10 due to the strongest interaction potential, as shown in Table 3. On the other hand, the overlapping effect of the molecule−pore wall interactions in the central position of the micropores of P20 and P25 is not enough for SO_2 to be filled; SO_2 molecules can be adsorbed only on the pore wall. However, the interaction potential of SO_2 with the graphitic slit pore is in the range of 985 to 1253 K, which is not sufficiently large compared with the thermal energy at the adsorption temperature (303 K). Hence, we must take into account the intermolecular interaction. The lateral interaction of Ψ_1 of SO_2 was calculated using the LJ interaction and the Stockmayer potential, which is given by eq 7:[44]

$$\Psi_1 = 4\epsilon_{ff}[(\sigma_{ff}/r)^{12} - (\sigma_{ff}/r)^6] - (\mu_1\mu_2/r^3)g(\theta_1,\theta_2,\varphi_1-\varphi_2) \quad (7)$$

Here $\epsilon_{ff} = 252$ K and $\sigma_{ff} = 0.429$ nm are the LJ parameters for

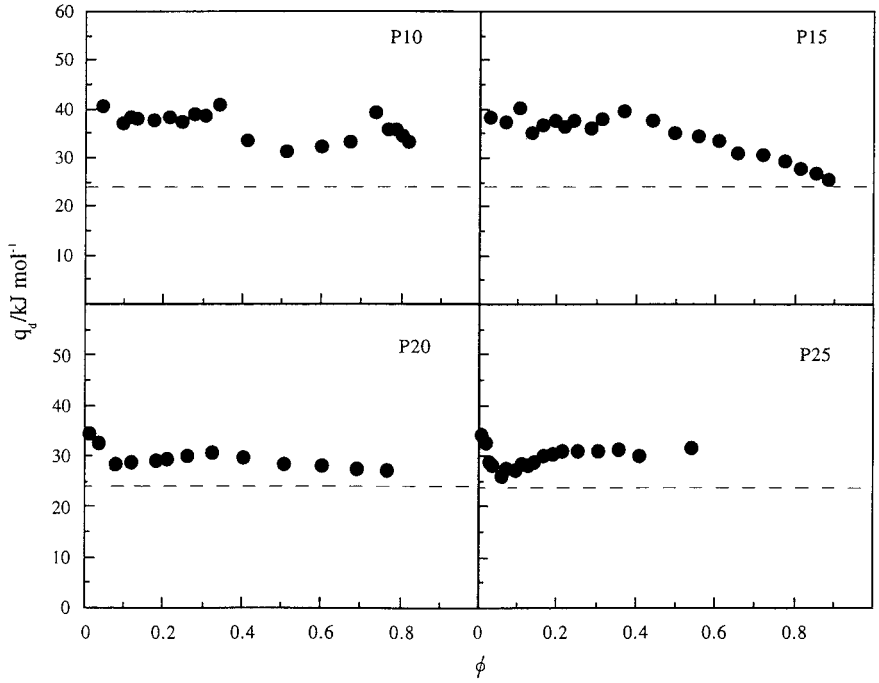

Figure 4. The differential adsorption energy of SO_2 on ACF samples.

TABLE 3: Calculation Results of Molecular Potential[a]

sample	P10	P15	P20	P25
w_m (nm)	0.79	1.01	1.13	1.45
z_m* (nm)	0.09	0.21	0.26	0.43
$\Psi(z_m^*)/k$ (K)	−1253	−1050	−1021	−985
$\Psi(z_m^*)/\Psi_0$	1.30	1.09	1.06	1.02
ratio of image interaction to $\Psi(z_m^*)$	0.25	0.28	0.32	0.31
Ψ_l/k (K)				
parallel	−42	−202	−38	−9
antiparallel	−362	−262	−104	−136
Ψ_{whole}/k (K)				
parallel	−1295	−1252	−1059	−994
antiparallel	−1302	−1018	−798	−816

[a] Here $\Psi_0/k = 963$ K.

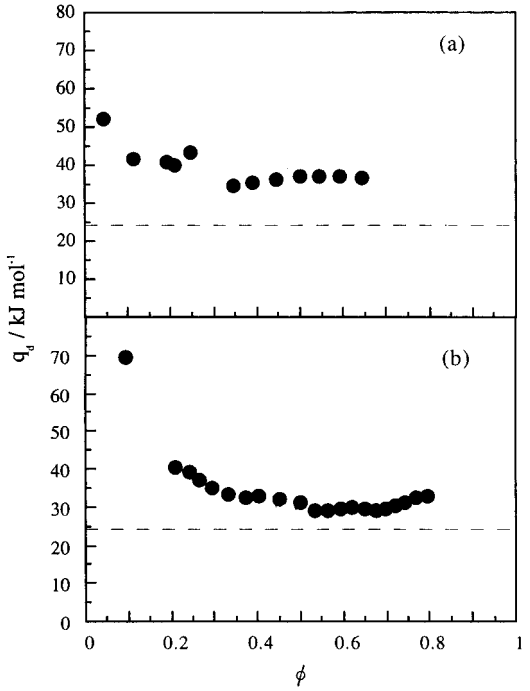

Figure 5. The differential adsorption energy of SO_2 on (a) AC and (b) BA.

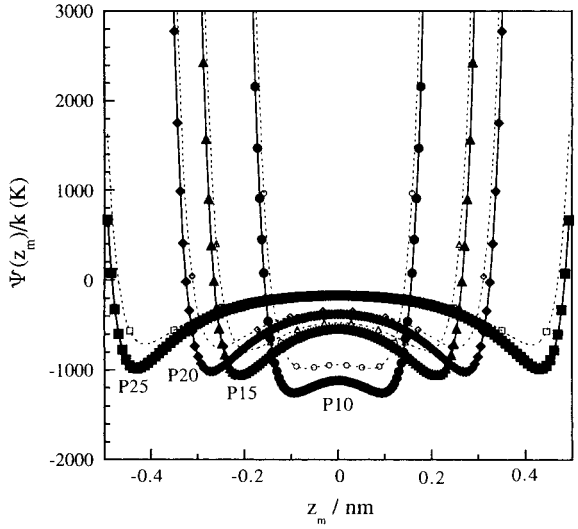

Figure 6. The interaction potential profile of SO_2 in micropores of P10, P15, P20, and P25: solid line, with image potential; broken line, without image potential.

SO_2 and $\mu_1 = \mu_2 = \mu = 1.61$ D (dipole moment); $g(\theta_1,\theta_2,\varphi_1-\varphi_2)$ is the angle dependence of the dipole−dipole interaction. θ_1, θ_2, and $\varphi_1-\varphi_2$ denote the molecular orientation of the dipoles; that is, θ_1 and θ_2 are the angles of the dipole moments of molecule 1 and molecule 2 to the axis directed from molecule 1 to molecule 2, respectively, and $\varphi_1-\varphi_2$ is the shadow angle of the dipole moments of molecule 1 and molecule 2 in the plane perpendicular to the axis directed from molecule 1 to molecule 2. We calculated the lateral interaction energies for the parallel and antiparallel orientations. To compare the experimental adsorption energy for SO_2 at the fractional filling ϕ, where the strong interaction of the dipole with the local electric field can be neglected and the contribution by the lateral interaction is not substantial, the whole potential energy including both the molecule−pore interaction and lateral interaction at $\phi = 0.4$ was calculated. The lateral interaction was obtained assuming uniform distribution of SO_2 molecules on the pore wall. Here the intermolecular distance was calculated from the amount of adsorption. In the case of P5 and P10, the bilayer adsorption does not occur owing to steric hindrance. Accordingly, we calculated the lateral interaction for molecules situated at the central position of the slit pore. With wider pores of P15, P20, and P25, we calculated the interaction energy for adsorption states that molecules occupy at the double minima, that is, monolayer adsorption on each pore wall. In the above calculation, we used the Stockmayer potential for the lateral interaction. As an SO_2 molecule has partial charges of +0.45 and −0.225 e at sulfur and oxygen atoms, respectively, the lateral interaction was calculated with the point charge model for the parallel and antiparallel cofigurations, too. The maximum difference between both models was 40 K, being unimportant in the total potential energy. Hence, only the lateral interaction energies by the Stockmayer potential calculation are shown here. In the future, molecular simulation should be more helpful. The calculated results are shown in Table 3. The absolute value of the whole potential energy, Ψ_{whole}, for the parallel orientation is larger than that for the antiparallel orientation other than P10. The whole potential energy for antiparallel orientation is higher than that for parallel orientation in the case of P10; the difference is only 7 K. Furthermore, the difference for other ACFs is 100−230 K at most. Hence, the orientation of the dipoles should not be ordered at 303 K, being completely different from the case for P5. The SO_2 molecules especially have no ordered structure in micropores of P10. On the other hand, some SO_2 molecules have a parallel orientation at $\phi = 0.4$ in micropores of P15, P20, and P25. If we used the total interaction energy including the lateral interaction energy, the differential adsorption energy at $\phi = 0.4$, $q_{d(a)}$, was calculated as shown in Table 4. The $q_{d(a)}$ values are closed to the observed values of $q_{d,\phi=0.4}$; q_d decreases with an increase of the pore width. The above molecular potential approaches can describe basically the adsorption states of SO_2 in the micropores of different pore widths. Hence, it

TABLE 4: Comparison of Calculated and Experimental Adsorption Energies of SO_2 in a Micropore

sample	(P5)	P10	P15	P20	P25
w_m/nm	(0.75)	0.79	1.01	1.13	1.45
$q_{d,(a)}$/kJ mol^{-1}	(37.8)	35.1	29.4	28.6	27.5
$q_{d,\phi=0.4}$/kJ mol^{-1}	(37 ± 2)	33 ± 2	36 ± 2	29 ± 2	30 ± 2

was shown that the ordering of the SO_2 dipoles sensitively depends on the pore width from the direct calorimetry and molecular potential calculation.

Acknowledgment. We are indebted to Dr. S. Hagiwara (Tokyo Richo Co.) for valuable comments. Dr. J. Fukazawa gave us Boehmite samples. This work was supported by a grant-in-aid for Scientific Research on Priority Areas No. 288 (Carbon Alloys).

References and Notes

(1) Dubinin, M. M. *Q. Rev. Chem. Soc.* **1955**, *9*, 101.
(2) Bering, B. P.; Dubinin, M. M.; Serpinsky, V. V. *J. Colloid Interface Sci.* **1966**, *21*, 378.
(3) Gregg, S. J.; Sing, K. S. W. *Adsorption, Surface Area and Porosity*, 2nd ed.; Academic: London, 1982; Chapter 4.
(4) Marsh, H. *Carbon* **1987**, *25*, 49.
(5) McEnaney, B. *Carbon* **1988**, *26*, 267.
(6) Rodriguez-Reinoso, F.; Molina-Sabio, M.; Munecas, M. A. *J. Phys. Chem.* **1992**, *30*, 593.
(7) Stoeckli, H. F. *Carbon* **1981**, *19*, 325.
(8) Jaroniec, M.; Gilpin, R. K.; Kaneko, K.; Choma, J. *Langmuir* **1991**, *7*, 2719.
(9) Everett, D. H.; Powl, J. C. *J. Chem. Soc., Faraday Trans. 1* **1976**, *72*, 619.
(10) Young, D. M.; Crowell, A. D. *The Physical Adsorption of Gases*; Butterworth: London, 1962; Chapter 9.
(11) Kiselev, A. V. *Discuss. Faraday Soc.* **1965**, *40*, 205.
(12) Beebe, R. A.; Dell, R. M. *J. Phys. Chem.* **1955**, *59*, 746.
(13) Masuda, T.; Tsutsumi, K.; Takahashi, H. *J. Colloid Interface Sci.* **1980**, *77*, 238.
(14) Pope, C. G. *J. Phys. Chem.* **1984**, *88*, 6312.
(15) Pope, C. G. *J. Phys. Chem.* **1986**, *90*, 835.
(16) Wojsz, R. *Pol. J. Chem.* **1989**, *63*, 233.
(17) Dubinin, M. M.; Isirikyan, A. A. *Izv. Akad. Nauk SSSR, Ser. Khim.* **1989** (10), 2183.
(18) Thamm, H. *J. Phys. Chem.* **1987**, *91*, 8.
(19) Thamm, H. *J. Phys. Chem.* **1988**, *92*, 193.
(20) Atkinson, D.; Carrott, P. J. M.; Grillet, Y.; Rouquerol, J.; Sing, K. S. W. *Fundamentals of Adsorption*; Liapis, A. I., Ed.; Engineering Foundation: New York, 1987; p 89.
(21) Kreiner, K.; Anielski, J. *Pol. J. Chem.* **1988**, *62*, 847.
(22) Rychlicki, G. *Pol. J. Chem.* **1989**, *63*, 255.
(23) Denoyol, R.; Fernandez-Colinas, J.; Grillet Y.; Rouquerol, J. *Langmuir* **1993**, *9*, 515.
(24) Alvarez, M. R.; Orralvo, M. J.; Grillet, Y.; Rouquerol, J. J. *Thermal Anal.* **1992**, *38*, 603.
(25) Davini, P. *Carbon* **1990**, *28*, 565.
(26) Moreno-Castilla, C.; Carrasco-Marin, F.; Vtrera-Hidalgo, E.; Rivera-Vtrilla, J. *Langmuir* **1993**, *9*, 1378.
(27) Seaton, N. A.; Walton, J. R. P.; Quirke, N. *Carbon* **1989**, *27*, 853.
(28) Balbuena, P. B.; Gubbins, K. E. *Fluid Phase Equilib.* **1992**, *76*, 21.
(29) Ball, P. C.; Evans, R. *J. Chem. Phys.* **1988**, *89*, 4412.
(30) Suzuki, T.; Kaneko, K.; Setoyama, N.; Maddox, M.; Gubbins, K. *Carbon* **1996**, *34*, 909.
(31) Iiyama, T.; Nishikawa, K.; Otowa, T.; Kaneko, K. *J. Phys. Chem.* **1995**, *99*, 10075.
(32) Kaneko, K. *Colloids Surfaces* **1996**, *109*, 319.
(33) Kakei, K.; Ozeki, S.; Kaneko, K. *J. Chem. Soc., Faraday Trans.* **1990**, *86*, 371.
(34) Kuwabara, H.; Suzuki, T.; Kaneko, K. *J. Chem. Soc., Faraday Trans.* **1991**, *87*, 1915.
(35) Suzuki, T.; Takahiro, K.; Kaneko, K. *Chem. Phys. Lett.* **1992**, *191*, 569.
(36) Setoyama, N.; Ruike, M.; Kasu, T.; Suzuki, T.; Kaneko, K. *Langmuir* **1993**, *9*, 2612.
(37) Kaneko, K.; Ishii, C.; Ruike, M.; Kuwabara, H. *Carbon* **1992**, *30*, 1075.
(38) Kaneko, K.; Shimizu, K.; Suzuki, T. *J. Chem. Phys.* **1992**, *97*, 8705.
(39) Setoyama, N.; Li, G.; Kaneko, K.; Okino, F.; Ishikawa, R.; Kanda, M.; Touhara, H. *Adsorption* **1996**, *2*, 293.
(40) Wang, Z.-M.; Kaneko, K. *J. Phys. Chem.* **1995**, *99*, 16714.
(41) Fukasawa, J.; Tsutsumi, H.; Sato, M.; Kaneko, K. *Langmuir* **1994**, *10*, 2718.
(42) Imai, J.; Kaneko, K. *Langmuir* **1992**, *8*, 1695.
(43) Steele, W. A. *Surf. Sci.* **1973**, *36*, 317.
(44) Hirschfelder, J. O.; Curtis, C. F.; Bird, R. B. *Molecular Theory of Gases and Liquids*; John Wiley: New York, 1964.
(45) Crowell, A. D. *J. Phys. Chem.* **1968**, *49*, 892.
(46) Linsen, B. G., Ed. *Physical and Chemical Aspects of Adsorbents and Catalysts*; Academic Press: London, 1970; Chapter 1.
(47) Kawazoe, K.; Kawai, T.; Eguchi, Y.; Itoga, K. *J. Chem. Eng. Jpn* **1974**, *7*, 157.